Chapter 4: Time-Dependent Indentation

The effects of time-dependent deformation on indentation experiments are considered in both analytical and experimental frameworks. Two different analytical approaches are considered, elastic-viscoelastic correspondence operations and an empirical viscous-elastic-plastic model. Experimental results are presented for indentation testing on time-dependent materials, including mineralized tissues bone and dentin.

4.1 Time-Dependent Effects in Indentation Testing

This section will focus on the demonstration of time-dependent mechanical behavior as seen during indentation testing under load-controlled conditions. Examples of time-dependent behavior experimental results are shown here for polymeric and biological materials.

4.1.1 Hallmarks of Indentation Creep

Nanoindentation has developed into a standard technique for measurement of local properties of engineering materials. This has been due in part to the availability of commercial instruments for small-scale contact testing along with the development of a standard analytic technique for mechanical property deconvolution (the "Oliver-Pharr" method). This technique relies on a mechanical response which is time-independent in the experimental timeframe.

Because of the capability for localized testing, nanoindentation testing is particularly well-suited to the analysis of biological materials, whose properties can vary substantially from point to point [Cuy et al, 2002]. This property variation may be based on variations in local composition, microstructure, and cell activity. However, the time-dependent nature of many biological materials has led to questions about the use of DSI for testing and analysis of these tissues.

The measured mechanical behavior of time-dependent materials depends on the experimental time frame utilized in the material characterization, as described in this work as the experimental "rise time", t_R. During a load-controlled nanoindentation test, creep is frequently observed in three ways, which will be illustrated here for indentation tests conducted on a time-dependent polymer (PMMA): (i) increasing displacement during a holding period at fixed peak load (Figure 4-1); (ii) forward-displacing creep during unloading such that the maximum displacement does not occur at peak load

(Figure 4-2); (iii) different load-displacement responses resulting from loading at different rates (Figure 4-3). Various schemes for trying to minimize time-dependent effects in indentation have been proposed, most centered on trying to "exhaust" the creep with a long holding time at peak load, in an attempt to obtain purely elastic (*e.g.* creep-unaffected) unloading in order to use the Oliver-Pharr deconvolution scheme [Briscoe et al, 1998; Feng and Ngan, 2002].

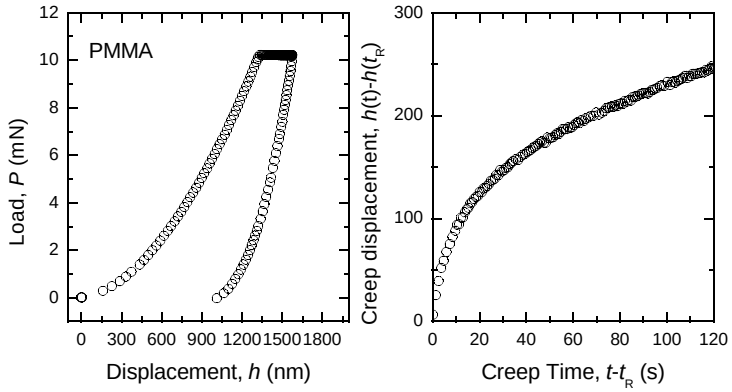

Figure 4-1: Indentation load-displacement (*P*-*h*) and creep-displacement-time (*h*-*t*) responses for PMMA at peak load (P_{max}) 10 mN.

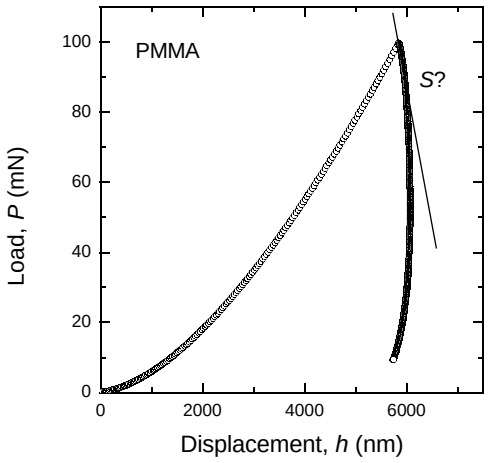

Figure 4-2: Indentation load-displacement (*P*-*h*) responses for PMMA conducted at slow rate (long rise time) to illustrate forward-displacing creep on unloading, and thus apparently negative stiffness (*S*)

Experimentally observed creep introduces errors when traditional elastic-plastic (Oliver-Pharr) analysis of nanoindentation data is used and time-dependence is ignored. In particular, forward-displacing creep negates the assumption in Oliver-Pharr that the slope of the unloading response is purely elastic recovery. Creep during unloading can increase the unloading slope, artificially increasing the perceived stiffness and in turn the calculated elastic modulus. In extreme cases, the unloading stiffness becomes negative because the creep displacement is greater in magnitude than the elastic recovery (Figure 4-2).

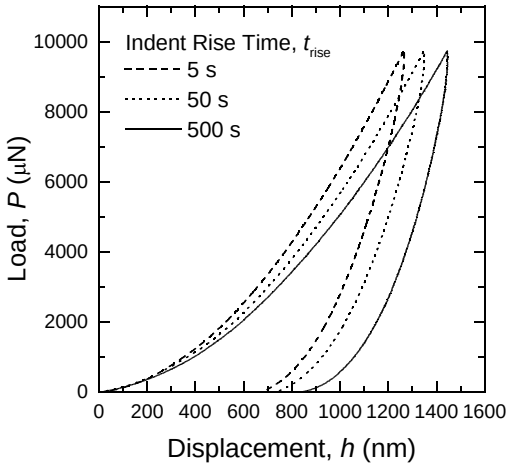

Figure 4-3: Indentation load-displacement (*P*-*h*) responses for PMMA conducted to peak loads (P_{max})of 10 mN at rise times (t_R) of 5, 50, and 500 s.

Time-dependent deformation also affects perceived values of the contact hardness, resulting in contact hardness values that appear smaller for slower loading rates (Figure 4-4). The smaller contact hardness values are not just an artifact of the deconvolution process, but correspond to increased size of the indentation residual impression. This is shown in Figure 4-5 for indentation tests at three different loading rates on the same polymeric material. As the impression area is in the denominator of the equation for contact hardness (Eqn. 3-12), physically larger residual impressions are associated with smaller contact hardness values.

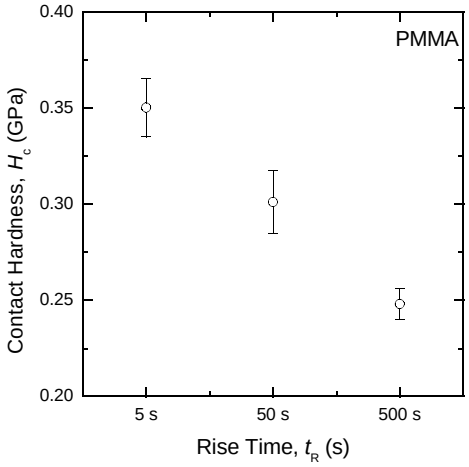

Figure 4-4: Contact hardness (H_c) deconvoluted from PMMA indentation traces conducted to peak loads (P_{max}) of 10 mN at rise times (t_R) of 5, 50, and 500 s. The perceived hardness decreases with slower loading,

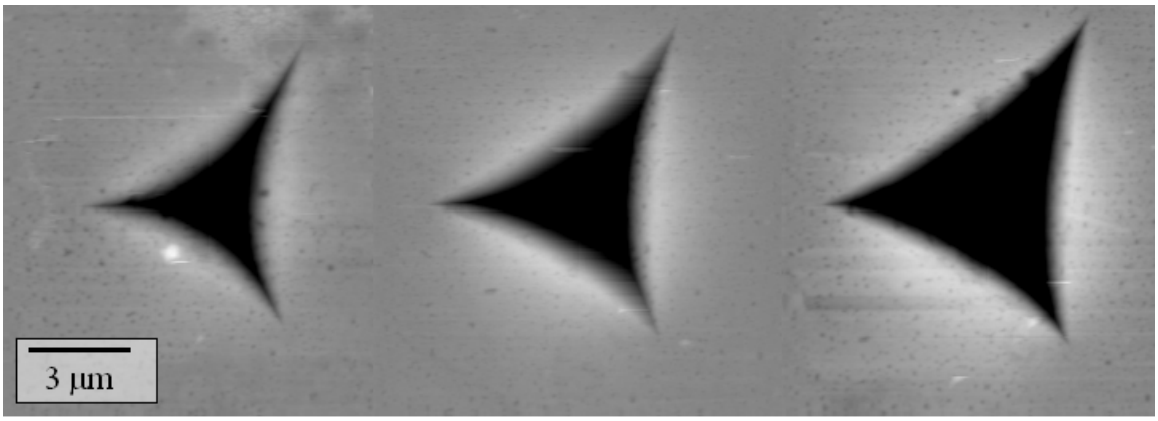

Figure 4-5: Residual impressions for indentation tests on PMMA, performed at rise times (t_R) of (left) 5 s, (center) 50 s, and (right) 500 s. There are changes in both the size and shape of the impression for different rise times.

Examples of time-dependent indentation behavior in mineralized tissues will be presented next.

4.1.2 Indentation Creep in Mineralized Tissues

Indentation creep in dry bone is shown in Figure 4-6 for tests conducted with a Berkovich indenter tip, under loading to 100 mN in 20 seconds and holding for creep for two minutes. The creep displacement is about 300 nm for each test, which is equal to approximately 10% of the total deformation during loading.

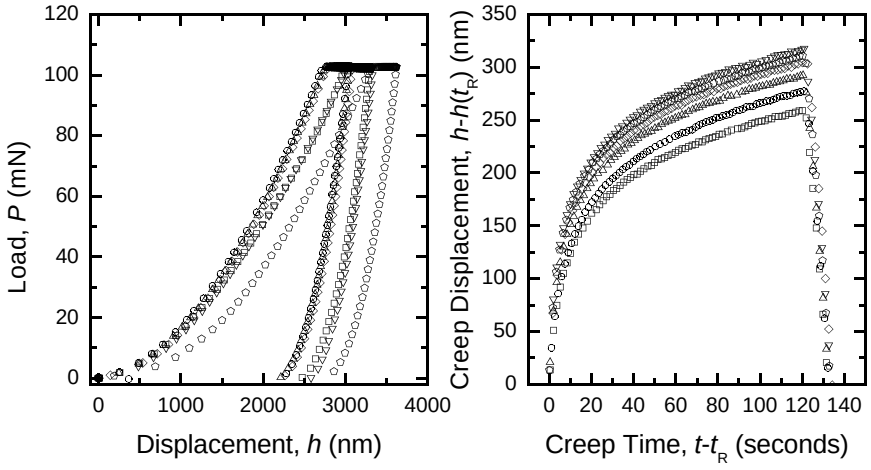

Figure 4- 6: Bone creep test (left) load-displacement (*P*-*h*) respose with peak load (P_{max}) 100 mN, and rise time (t_R) 20 s; (right) creep displacement-creep time response during the 120 s holding period.

Rate-dependence was evaluated in dry dentin by conducting indentation tests at different rates. Tests were performed in duplicate to peak load levels of 10 mN with rise times of 30, 100, and 300 seconds. The experimental load-displacement traces are illustrated in Figure 4-7 (left). Time-dependence in the indentation response is present even in the dehydrated dentin tissue. The time-dependence and its effect on the shape of the indentation responses can be examined in more detail by normalizing the load-displacement (*P*-*h*) curves by the peak point $\{h(P_{max}), P_{max}\}$. The changes in the unloading response due to time-dependence are then clearly visible (Figure 4-7, right).

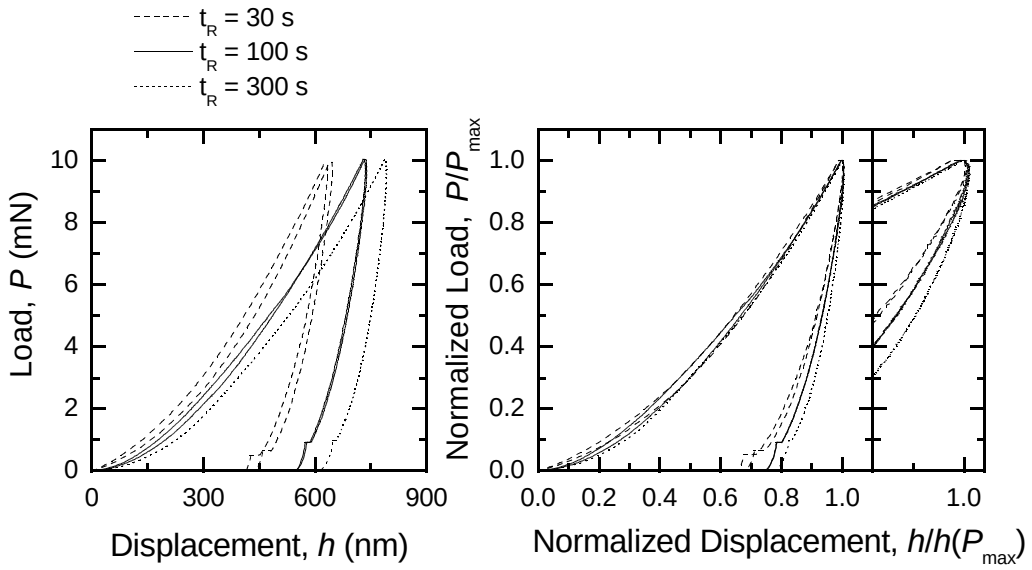

Figure 4-7: (left) Dry dentin indentation load-displacement (*P*-*h*) responses for constant loading rate indentation tests at three different loading rates (rise times). The total displacement increases with longer rise time. (right) Normalized indentation responses ($h/h(P_{max})$, P/P_{max}) for dry dentin responses seen in on the right. Differences in unloading curve shape with rate are evident on the normalized plot (especially in the zoomed region at far right). The unloading response is steeper for larger values of the rise time (t_R) corresponding to slower loading.

Although the examples presented in Figures 4-1 to 4-7 demonstrate time-dependent mechanical behavior during indentation testing conditions, until recently insufficient methodologies have existed for quantitative examination of indentation testing in time-dependent materials, with the exception of the primitive model-independent measures discussed in section 2.2.1. Explicit viscoelastic models for indentation have been the focus of much recent research [Cheng et al, 2000; Sakai and Shimizu, 2001; Lu et al, 2003; Oyen and Cook, 2003; Oyen, 2005] and will be discussed at length next in this chapter.

4.2 Viscoelastic Indentation by Radok Correspondence

In the case of an elastic indentation problem, there is a closed-form analytical solution for the load-displacement behavior. As was discussed in Chapters 2 and 3, the relationship between load (P) and displacement (h) is not linear, with $P \sim h^{3/2}$ for spherical indentation and $P \sim h^2$ for conical-pyramidal indentation. Lee and Radok [1960] proposed in a landmark paper that a pseudo-linear viscoelastic analysis could be performed for the indentation problem by replacing the elastic constants within the nonlinear load-displacement relationship with viscoelastic operators. In the simplest case, when the material is incompressible ($\nu = 0.5$), the first approximation to the viscoelastic problem is quite simple. The approach is actually quite similar to the "Quasi-Linear Viscoelastic" (QLV) analysis frequently employed for time-dependence in soft biological tissues [Fung, 1993]. Correspondence analysis has been used to examine indentation with a Standard Linear Solid model for a flat punch [Cheng et al, 2000] or spherical indenter tip [Cheng et al, 2005], and for a variety of tip geometries using a Maxwell material model [Sakai and Shimizu, 2001]. In the current work, conical and spherical indentation conditions are examined for viscoelastic materials in general, followed with an analysis is developed for multiple time-constant material models with an emphasis on loading conditions more experimentally attainable than the step-loading creep assumption used by Cheng et al [2005].

4.2.1 Nonlinearly Viscoelastic Indentation Mechanics

The relationship between the elastic modulus (E) and shear modulus (G) for and incompressible, isotropic elastic material is:

$$G = \frac{E}{2(1+\nu)} = \frac{E}{3} \qquad [4\text{-}1]$$

and the indentation (plane strain) modulus is:

$$E' = \frac{E}{(1-\nu^2)} = 4\frac{E}{3} = 4G \qquad [4\text{-}2]$$

Recalling the elastic solution for a spherical indenter (Hertzian contact)

$$h^{3/2} = \frac{3}{4\sqrt{R}} P \frac{(1-\nu^2)}{E} \qquad [4\text{-}3]$$

and replacing the plane strain modulus with the shear modulus gives:

$$h^{3/2} = \frac{3P}{16G\sqrt{R}} \qquad [4\text{-}4]$$

Similarly, the elastic solution for a conical (or pyramidal) indenter is:

$$h^2 = \frac{2\gamma^2}{\pi \tan\psi} P \frac{(1-\nu^2)}{E} \qquad [4\text{-}5]$$

which can be written in terms of the shear modulus for an incompressible material as:

$$h^2 = \frac{P\gamma^2}{2\pi G \tan\psi} \qquad [4\text{-}6]$$

For viscoelastic correspondence under load-control (as in indentation testing) $P/2G$ is replaced in the elastic solution [Johnson, 1985] with an integral operator for load-control:

$$\left[\frac{P}{2G}\right] \rightarrow \int_0^t J(t-t')\frac{\mathrm{d}P(t')}{\mathrm{d}t'}dt' \qquad [4\text{-}7]$$

where $J(t)$ is the shear creep compliance for the material [Lee and Radok, 1960]. The elastic solutions for spherical and conical indentation can be rewritten as:

$$h^{3/2} = \frac{3}{8\sqrt{R}}\left[\frac{P}{2G}\right] \qquad [4\text{-}8]$$

$$h^2 = \frac{\gamma^2}{\pi \tan\psi}\left[\frac{P}{2G}\right]$$

and then , in terms of the viscoelastic operator,

$$h^{3/2} = \frac{3}{8\sqrt{R}}\int_0^t J(t-t')\frac{\mathrm{d}P(t')}{\mathrm{d}t'}dt' \qquad [4\text{-}9]$$

$$h^2 = \frac{\gamma^2}{\pi \tan\psi}\int_0^t J(t-t')\frac{\mathrm{d}P(t')}{\mathrm{d}t'}dt'$$

The hereditary integrals can then be solved for any set of loading conditions, including creep at fixed load following a step load, ramping at constant loading rate, and creep following ramp loading at constant loading rate. A key issue with this Lee and Radok [1960] correspondence analysis, particularly relevant to the indentation problem, is the requirement that the contact are be non-decreasing. Therefore, the unloading segment of the indentation test cannot be solved using this analysis, but loading and creeping segments can.

For the simplest case, creep following a step load, the load input is $P(t') = P_0 H(t')$ where $H(t)$ is the Heaviside step function. In this case, the term $[P/2G]$ becomes simply $P_0\, J(t)$ after integration, and the creep displacement for spherical indentation is:

$$h^{3/2}(t)=\frac{3P_0}{8\sqrt{R}}J(t)$$

The instantaneous (zero-time) shear modulus G can be found by

$$G=\frac{1}{2J(0)} \qquad [4\text{-}10]$$

where the factor of two arises because of the definition of shear and normal strains [Lee and Radok, 1960; Johnson, 1985].

For the standard linear solid model (Figure 2.18iii) the creep compliance function is (Eqns 2-28, 2-29):

$$J(t)=\frac{1}{g_1}+\frac{1}{g_2}\left(1-\exp(-t/\tau_C)\right) \quad \text{where} \quad \tau_C=\eta/g_2 \qquad [4\text{-}11]$$

Using this standard linear solid model, the practical implementation of the correspondence analysis for creep data is simple. After raising the displacement data to the appropriate power, the creep data can be fit to an exponential decay function for creep of the form:

$$h^n(t)=B-C\exp(-t/\tau_C) \qquad [4\text{-}12]$$

where n = 3/2 for Hertzian, n = 2 for Berkovich. Abbreviating the indentation geometry constants k_G where:

$$k_G=\frac{3}{16\sqrt{R}} \text{ for Hertzian} \qquad [4\text{-}13]$$

$$k_G = \frac{\gamma^2}{2\pi \tan\psi} \quad \text{for Berkovich} \qquad [4\text{-}14]$$

the fitting parameters are simply related to the material constants:

$$B = k_G P_0 \left(\frac{1}{g_1} + \frac{1}{g_2} \right) \qquad [4\text{-}15]$$

$$C = k_G P_0 \frac{1}{g_2} \qquad [4\text{-}16]$$

The shear modulus can be found by

$$G = \frac{1}{2J(0)} = \frac{g_1}{2} \qquad [4\text{-}17]$$

The process of calculating the shear modulus is similar for generalized creep compliance functions with more than one time-constant (Eqn. 2-30).

4.2.2 Creep Following Ramp Loading

An important analysis is for the creep test following ramp loading instead of an experimentally unattainable step load, which is easily solved following integration utilizing the Boltzmann hereditary integral.

For a ramp from zero load to a peak load for a creep test, the loading conditions can be written:

$$P(t) = k\,t \;, \qquad 0 \le t \le t_R \qquad [4\text{-}18]$$

$$P(t) = P_{max} = k\,t_R \;, \qquad t \ge t_R \qquad [4\text{-}19]$$

The hereditary integral (eqn. 4-9) must be solved twice, for the ramp (eqn. 4-18) and hold (eqn. 4-19):

$$h^{3/2}(t)=\frac{3}{8\sqrt{R}}\int_0^t J(t-u)\,k\,du\ , \qquad 0\le t\le t_R \qquad [4\text{-}20]$$

$$h^{3/2}(t)=\frac{3}{8\sqrt{R}}\left[\int_0^{t_R} J(t-u)\,k\,du+\int_{t_R}^{t} J(t-u)\,0\,du\right]=\frac{3}{8\sqrt{R}}\int_0^{t_R} J(t-u)\,k\,du\ ,\ t\ge t_R \qquad [4\text{-}21]$$

The solutions to these integral equations are completely dependent on the choice of material creep function $J(t)$ over which the integration is conducted. Solution of eqns. 4-20 and 4-21 for the creep function given by eqn. 2-30 gives

$$h^{3/2}(t)=\frac{3k}{8\sqrt{R}}\left[C_0 t-\sum C_i\tau_i\left(1-\exp(-t/\tau_i)\right)\right]\ , \quad 0\le t\le t_R \qquad [4\text{-}22]$$

$$h^{3/2}(t)=\frac{3k}{8\sqrt{R}}\left[C_0 t_R-\sum C_i\tau_i\exp(-t/\tau_i)\left(\exp(t_R/\tau_i)-1\right)\right]\ ,\ t\ge t_R \qquad [4\text{-}23]$$

Eqn. 4-23 for the creep segment can be directly fit to the data to obtain parameter values, and the ramp and hold segments (Eqns. 4-22 and 4-23) can be repredicted.

This procedure is illustrated in Figure 4-8 for indentation tests on PL-1 polymer for indentation creep tests performed to 100 mN peak load with rise times of 20, 50, 100, and 200 seconds and an indenter tip radius of 150 μm. The creep data from the 20 s rise time were fit to eqn. 4-23 using a two time-constant relaxation function and the full response was predicted from the obtained parameters and Eqns. 4-22 and 4-23. The responses from the three other rise times were then predicted from the parameters obtained from the fit to the 20 s rise time data. There is excellent predictive capability for the slower rise times. The creep-portion of the data from Figure 4-8 are shown in Figure

4-9 on an expanded scale, where the displacement and time have been reset to zero at the start of the holding period. The solid lines are the predictions from Figure 4-8.

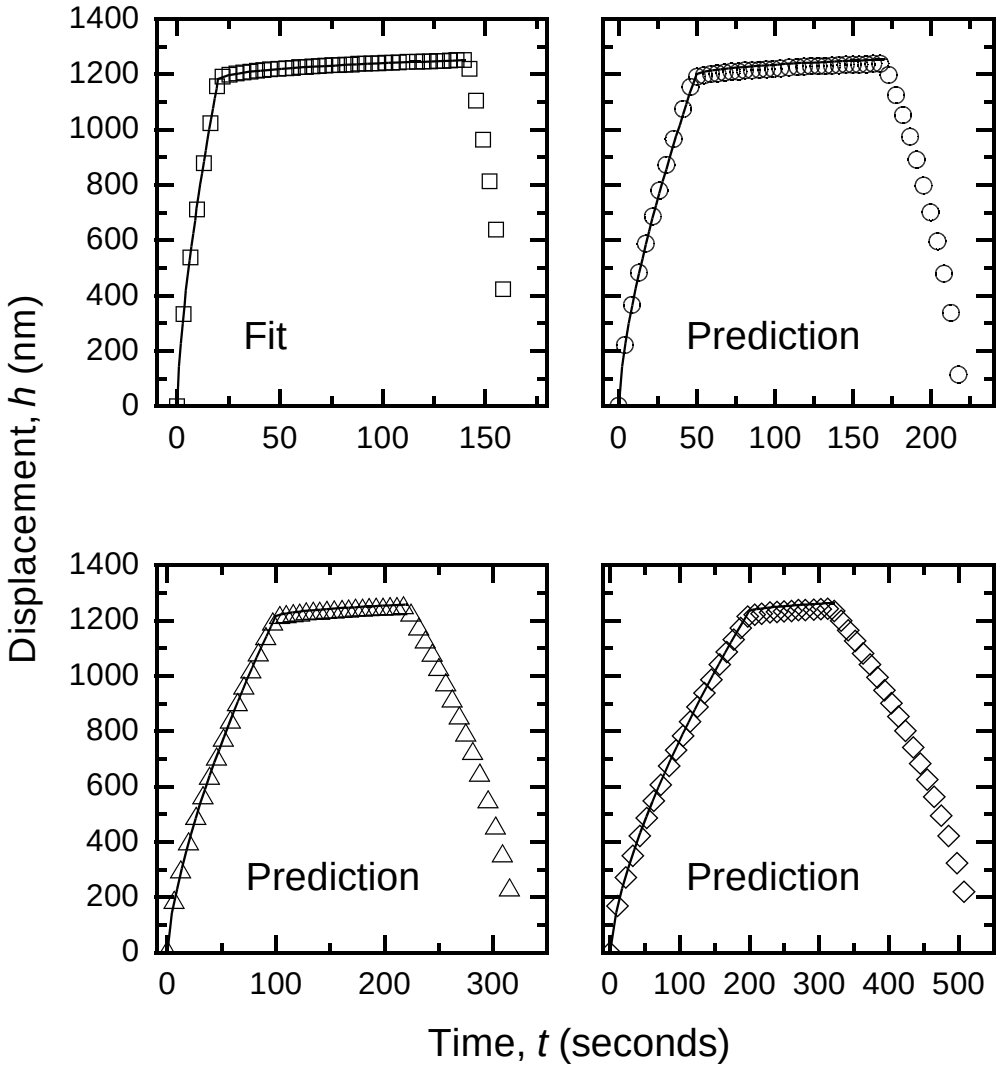

Figure 4-8: PL-1 polymer indentation ramp-and-hold creep displacement-time (*h*-*t*) experimental data (open symbols) for loading to 100 mN at four different loading rates. The solid lines are fits and predictions from Eqns. 4-22 and 4-23 as marked, using a two-time constant relaxation function.

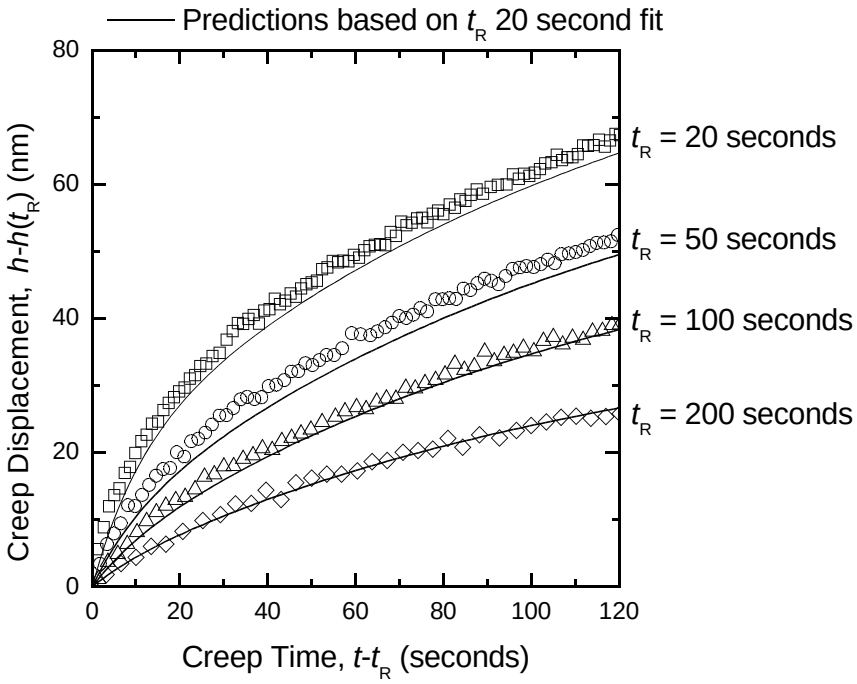

Figure 4-9: Creep displacement-time (*h*-*t*) data from the load-hold portion of the PL-1 polymer data shown in Fig. 4-8. Predictions for the creep displacement are shown as solid lines on the graph.

The shear modulus (*G*) value obtained from the parameters was 1.3 GPa, in good agreement with the known value of 1.1 GPa. Spherical indentation has great promise in eliminating the uncertainties and unknown effects associated with the elevated modulus seen in Berkovich indentation of polymers (Section 3.1.2.2).

The results presented here were for spherical indentation using a very large radius indenter tip on a polymeric material. For spherical indentation, especially if the spherical indenter tip is large relative to the depth of the indent, this analysis is itself sufficient as the deformation can be restricted to purely elastic or viscoelastic. In the case of Berkovich indentation there is time-independent plastic deformation on loading in all materials but elastomers. Therefore, the use of Radok correspondence for pyramidal indentation testing is not very practicable in most experiments. However, most

indentation tests at nano- to micro-scale are typically performed with sharp, pyramidal indenters such as a Berkovich or cube-corner, particularly because of the improved spatial resolution in measurements. Therefore, in the following section, conical/pyramidal indentation with combined viscous, elastic, and plastic deformation is considered and an empirical model is used to examine the time-dependent deformation in a glassy polymer.

4.3 The "VEP" Model

In this section, an empirical model for pyramidal indentation of viscous-elastic-plastic materials is briefly reviewed. (This model was co-developed by myself in previous research work.) A new procedure for fitting unloading data to obtain VEP parameters is then developed and tested for indentation tests on a polymeric material with known elastic modulus.

4.3.1 Model

As discussed previously, the load is proportional to the square of the displacement in conical-pyramidal indentation testing. The VEP model [Oyen and Cook, 2003] is an extensively framed model for time-dependent indentation based on quadratic elements developed in analogy to the linear elements classically associated with viscoelastic mechanical models. The elastic element, instead of a linear spring, is given by:

$$P_e = \alpha_2 E' h_e^2 \qquad [4\text{-}24]$$

where P_e and h_e are the load and displacement on the elastic element,where E' is the plane strain modulus of the material (Eqn 2-17) and α_2 is the dimensionless geometrical factor (obtained by comparison of Eqns 4-24 and 4-5) equal to 4.4 for a Berkovich indenter. Under indentation conditions, substantial plastic deformation can occur beneath the indenter. For a rigid, perfectly plastic material, a deformation element constrained by geometric similarity, appropriate to conical or pyramidal indentation is

$$P_p = \alpha_1 H h_p^2 \qquad [4\text{-}25]$$

where P_p and h_p are the load and displacement on the plastic element, H is the resistance

to plastic deformation (see Appendix B), and $\alpha_1 = \pi \tan^2 \psi$ is the dimensionless geometry parameter for a sharp indenter with effective included angle 2ψ, such that the value of α_1 is equal to 24.5 for a Berkovich indenter.

In direct analogy with the linear dashpot, a quadratic viscous constitutive response was chosen in which the load is proportional to the square of the displacement rate:

$$P_v = \alpha_2 E' \tau_Q^2 \left(\frac{\mathrm{d}h_v}{\mathrm{d}t} \right)^2 = \alpha_2 \eta_Q \left(\frac{\mathrm{d}h_v}{\mathrm{d}t} \right)^2 \qquad [4\text{-}26]$$

such that an empirical time constant can be defined as

$$\tau_Q = \sqrt{(\eta_Q / E')} \qquad [4\text{-}27]$$

A series combination of these three elements (viscous, elastic, plastic) is a direct extension of a linear Maxwell model but for geometrically-similar (quadratic) indentation conditions and including plasticity. This series assumption gives equal loads in the three elements and a total displacement arising from the sum of the displacements in the individual elements. Since the displacements sum, the displacement rates also sum, giving the VEP constitutive differential equation:

$$\frac{\mathrm{d}h}{\mathrm{d}t} = \frac{P^{1/2}}{(\alpha_2 \eta_Q)^{1/2}} + \frac{1}{2P^{1/2}} \frac{\mathrm{d}P}{\mathrm{d}t} \left[\frac{1}{(\alpha_2 E')^{1/2}} + \frac{1}{(\alpha_1 H)^{1/2}} \right] \qquad [4\text{-}28]$$

This constitutive relation can be solved for different loading conditions, and in particular for conditions used in indentation experiments, such as constant loading and unloading at fixed rates. In contrast to Radok correspondence (section 4.2) there is no restriction on the contact area increasing at all times, such that the unloading condition for a standard load-unload indentation test can be solved explicitly. For a loading segment under

constant loading rate (k) up to a peak load, P_{max}, at time t_R, the loading conditions can be represented as

$$P(t) = k\,t$$
$$\frac{\mathrm{d}P}{\mathrm{d}t} = k \quad \text{for} \quad 0 \le t \le t_R \qquad [4\text{-}29]$$

which upon insertion into the VEP constitutive equation (Eqn. 4-28) gives

$$\frac{\mathrm{d}h}{\mathrm{d}t} = \frac{(k\,t)^{1/2}}{(\alpha_2 \eta_Q)^{1/2}} + \frac{k^{1/2}}{2t^{1/2}}\left[\frac{1}{(\alpha_2 E')^{1/2}} + \frac{1}{(\alpha_1 H)^{1/2}}\right] \qquad [4\text{-}30]$$

This simple differential equation is solved to give:

$$h^{\mathrm{LOAD}}(t) = k^{1/2} t^{1/2}\left[\frac{2t}{3(\alpha_3 \eta_Q)^{1/2}} + \frac{1}{(\alpha_2 E')^{1/2}} + \frac{1}{(\alpha_1 H)^{1/2}}\right] \qquad [4\text{-}31]$$

For unloading from the peak load (P_{max}) at time $t = t_R$, for constant unloading rate ($-k$) equal to the negative of the constant loading rate, the loading input is defined by

$$P(t) = k\,t_R - k(t - t_R) = k(2t_R - t)$$
$$\frac{\mathrm{d}P}{\mathrm{d}t} = -k; \qquad t_R \le t \le 2t_R \qquad [4\text{-}32]$$

For unloading with perfect plasticity, the plastic element is suppressed such that $h_p = h_p^{max} = h_p(t_R)$ and thus $\mathrm{d}h_p/\mathrm{d}t = 0$. The unloading constitutive equation is thus truncated from Eqn. 4-28 to give

$$\frac{\mathrm{d}h}{\mathrm{d}t}=\frac{(k(2t_{\mathrm{R}}-t))^{1/2}}{(\alpha_2\eta_{\mathrm{Q}})^{1/2}}-\frac{1}{(k(t_{\mathrm{R}}-t))^{1/2}}\frac{k}{2(\alpha_2 E')^{1/2}} \qquad [4\text{-}33]$$

which is solved to give the unloading response for times greater than t_{R}:

$$h^{\mathrm{UNLOAD}}=\left[\frac{1}{(\alpha_2 E')^{1/2}}+\frac{1}{(\alpha_1 H)^{1/2}}+\frac{2t_R}{3(\alpha_2\eta_Q)^{1/2}}\right](kt_R)^{1/2}+\frac{1}{(\alpha_2 E')^{1/2}}\left[(2kt_R-kt)^{1/2}-(kt_R)^{1/2}\right]$$
$$-\frac{2}{3k(\alpha_2\eta_Q)^{1/2}}\left[(2kt_R-kt)^{3/2}-(kt_R)^{3/2}\right] \qquad [4\text{-}34]$$

Only for such non-monotonic loading (e.g. the combination of loading and unloading) is there is a distinction between the elastic and plastic elements, a situation which will be used in the next section in developing a technique for routine implementation of this model.

4.3.2 Adaptation of the VEP Model to Routine Testing

In the VEP unloading response (Eqn. 4-34), information to fit all three parameters is contained in this single equation: the unloading response initiates at a point depending on all three modes of deformation, but contains no further plastic deformation (this was fixed at P_{max}) and the unloading response is the competition between the elastic recovery and further viscous deformation. The usefulness of this unloading curve in examining pyramidal indentation of viscous-elastic-plastic materials was examined first using a polymer (PL-1).

Indentation tests were performed to different peak load levels (P_{max} = 0.3 to 300 mN) using fixed 30 second rise times (t_{R}) with four repeats per load level. The VEP unloading *h*-*t* solution (Eqn. 4-34) was fit to the experimental unloading data for each PL-1 polymer indentation trace using the nonlinear curve-fit function (Levenberg-Marquardt iterations) in a commercial analysis package (Microcal Origin 6.1, OriginLab,

Northampton, MA). A representative unloading displacement-time (*h*-*t*) fit is shown in Figure 4-10 (left) for a 100 mN indentation test. The modulus, hardness, and empirical viscosity properties (E', H, η_Q) were calculated from the numerical values of the dimensionless geometrical constants for a Berkovich indenter, $\alpha_2 = 4.4$ and $\alpha_1 = 24.5$. The time constant τ_Q was calculated from the modulus and viscosity terms as per Eqn 4-27. The full loading- and unloading response was generated from the VEP model (Eqns. 4-31 and 4-34) based on the properties obtained from the fit, and is shown as the solid line in Fig. 4-10 (right).

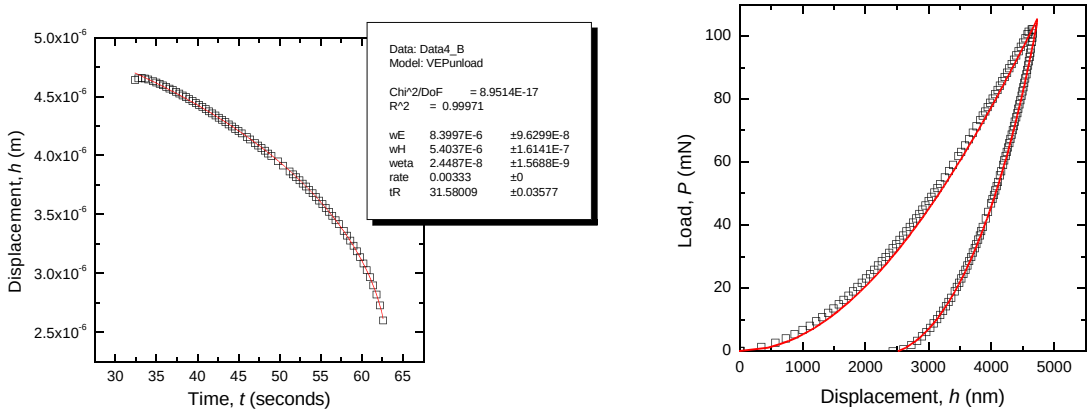

Figure 4-10: (left) Unloading displacement-time profile for PL-1 polymer indentation. The hollow symbols are experimental data and the line is the fit. (right) The full PL-1 experimental load-displacement (*P*-*h*) trace (hollow symbols) from same data shown on the left. The solid line is the full loading- and unloading response from VEP model, generated using the parameters obtained from the fit.

Following the fits for indentation tests at all peak load levels, parameters at each load level were averaged, standard deviations were calculated, and the numerical results are presented in Table 4- 1. There was a slight trend downward in elastic modulus with rise time, consistent with the data shown in Figure 3-9 from continuous stiffness measurements of the same PL-1 polymer in which the Oliver-Pharr modulus was a decreasing function of displacement. However, while the Oliver-Pharr modulus was

substantially elevated with respect to the tensile modulus (E ~ 3 GPa) the VEP values were comparable to the tensile modulus (Figure 4-15). The viscosity and time constant trended slightly upwards with peak load level, indicating less time-dependence in the response at greater depths. The resistance to plastic deformation (H) was very large at the smallest load levels (0.3, 1 mN), and was approximately fixed at about one third the surface value at larger peak loads.

Table 4-1: PL-1 properties from VEP fits. Means and standard deviations for four indentation tests per load level.

P_{max} (mN)	E (GPa)	H (GPa)	η_Q (TPa-s^2)	τ_Q (s)
0.3	3.63 ± 0.34	4.86 ± 2.17	100 ± 34	153 ± 21
1	3.40 ± 0.34	4.57 ± 3.95	87 ± 18	149 ± 9
3	3.69 ± 0.20	1.97 ± 0.37	140 ± 49	180 ± 26
10	3.43 ± 0.17	1.71 ± 0.25	131 ± 33	181 ± 19
30	3.05 ± 0.02	1.42 ± 0.07	138 ± 11	199 ± 8
100	2.72 ± 0.10	1.35 ± 0.04	187 ± 17	246 ± 16
300	2.50 ± 0.11	1.48 ± 0.10	160 ± 15	237 ± 14

Now that a protocol has been established for calculating VEP parameters from an unloading displacement-time data curve-fit, the method will be applied to examine indentation data for tests on mineralized biological tissues. I begin with a test case, to examine what should be an obvious change in time-dependent mechanical behavior, for comparisons of dry and hydrated dentin.

4.4 Time-Dependent Indentation Experiments on Mineralized Tissues

Indentation tests were performed at constant loading rates on both dry and wet dentin to examine the effect of hydration on VEP properties. Bone indentation responses for tests performed under identical conditions were then examined to establish the point-to-point variation in bone VEP properties.

4.4.1 VEP Analysis of Dentin Hydration

The effect of hydration on the indentation responses of dentin tissue was evaluated by performing tests on the same sample under identical indentation conditions (P_{max} = 10 mN, t_R = 100 s) in different hydration states: (1) as-received (from the freezer) dry dentin, (2) after soaking the tissue for one hour in distilled water, and (3) after allowing the sample to dehydrate in air for three hours following the rehydration.

Raw load-displacement traces for indentation tests on dentin in the three states of fluid hydration are shown in Figure 4-11. The dehydrated tests (stage (3) above) are similar to the original dry tests. The effect of hydration is two-fold: (i) the total displacement (at both P_{max} and at the end of the test) increases, and (ii) the variability in indentation responses also appears to increase.

Examination of these data in normalized coordinates illustrates the changes to indentation unloading response shape with hydration (Figure 4-12). The dehydrated (stage 3) traces have the same shape as the original dry traces, while the hydrated traces display a steeper unloading response compared to the non-hydrated traces. The responses for the three hydrated tests are all different.

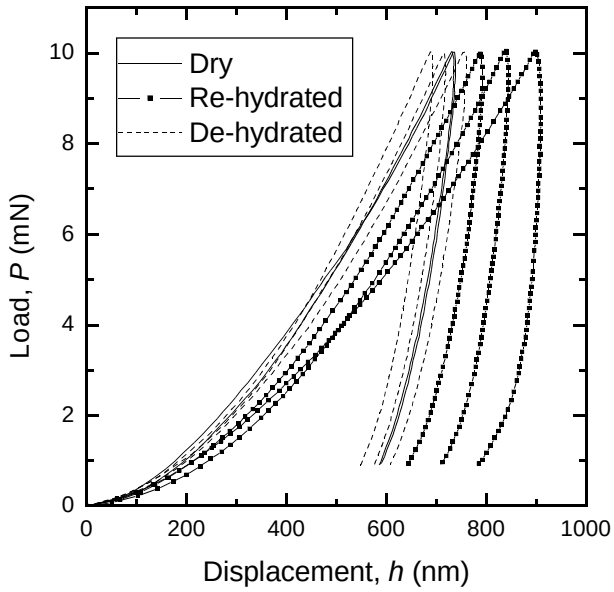

Figure 4-11: Indentation load-displacement (*P*-*h*) responses for dry dentin, after soaking in water, and after dehydrating in air after the wet-testing.

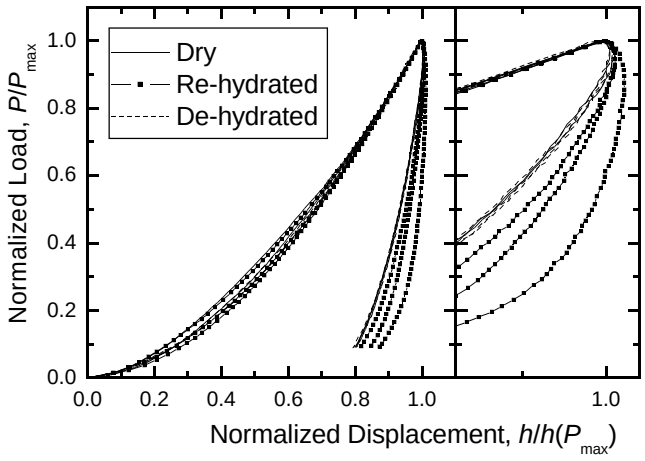

Figure 4-12: Normalized indentation responses ($h/h(P_{max})$, P/P_{max}) responses for dry dentin, after soaking in water, and after dehydrating in air following the wet-testing.

Table 4-2 contains the mean and standard deviation for mechanical properties obtained from the dentin load-displacement traces shown in Figs 4-16 . Both Oliver-Pharr (O-P) elastic-plastic deconvolution (section 2.1.4) and VEP time-dependent deconvolution (section 4.3.2) were separately employed to fit the unloading data and obtain property values, and are presented together here for comparative purposes.

Table 4-2: Mechanical properties deconvoluted from dentin indentation load-displacement traces using Oliver-Pharr deconvolution or the VEP model

	(1) dry	***(2) re-hydrated***	***(3) de-hydrated***
O-P Modulus, E' (GPa)	28.3 ± 0.2	42.9 ± 17.1	29.8 ± 2.4
O-P Contact Hardness, H_c (GPa)	0.87 ± 0.01	0.61 ± 0.11	0.89 ± 0.08
VEP Modulus, E' (GPa)	30.5 ± 1.3	21.6 ± 4.6	30.5 ± 1.6
VEP viscosity, $10^{-15}\eta_Q$ (Pa s^2)	7.8 ± 1.4	1.3 ± 0.8	6.3 ± 0.4
VEP Time Constant, τ (s)	505 ± 33	235 ± 65	453 ± 16
VEP Hardness, H (GPa)	2.18 ± 0.07	2.38 ± 0.49	2.39 ± 0.29

Interesting patterns emerge from examination of the numerical data. The dry (stage 1) and dehydrated (stage 3) data are comparable for all properties. For the Oliver-Pharr deconvolution, the elastic modulus results from the hydrated condition are likely affected by the unloading stiffness problems discussed above in section 4.1 such that the unloading slope does not represent purely elastic unloading, but a competition between elastic unloading and further viscous deformation. As such the elastic modulus is large and overstated, and thus the counterintuitive result for a substantially increased modulus with hydration. The O-P contact hardness data are more intuitive, with an approximately 30% decrease in contact hardness for hydrated samples compared with dry samples.

The VEP modulus results do not suffer from the problems associated with Oliver-Pharr deconvolution for hydrated tissue, and demonstrate about a 30% decrease in modulus for hydrated samples compared to dry samples. In the dry state, the VEP and OP modulus values are approximately equal.

VEP plastic deformation resistance (*H*) is unchanged in the three conditions. The time constants were approximately halved for the hydrated state, which relative to the rise time of 100s would give substantially increased viscous deformation. The VEP viscosity numbers reflect this trend towards more viscous behavior as well, with about five or six times lesser viscosity in the hydrated state compared to the dry state.

The drop in elastic modulus observed in this study was greater than has been noted in tensile testing of wet and dessicated dentin, for which the modulus of wet dentin was 15% lower than dry dentin [Huang et al, 1992]. The numerical values from tensile testing (15 and 18 GPa for wet and dry, respectively) were also substantially lower than those observed here for indentation which may reflect difficulties in the tensile testing method or apparatus for extremely small tooth samples. However, the decrease in yield stress with hydration in the tensile study [Huang et al, 1992] was 24%, comparable to the 30% decreases in O-P contact hardness seen in the current study, reassuring given that the contact hardness is reported to be directly related to yield stress, [Tabor, 1951].

4.4.2 VEP Analysis of Healing Bone

Next, the viscous-elastic-plastic (VEP) empirical indentation model was used to assess the point-to-point variability of properties in dry healing porcine bone. Constant loading- and unloading-rate depth-sensing indentation tests were performed at a constant loading rate (0.333 mN s^{-1}) to a peak load of 10 mN. A total of 75 separate indentation tests on bone samples from two animals with bone healing times of one month (Section 3.2.1) were analyzed for the current study. Spatial position was recorded for each indentation test and approximate distance from the implant interface was calculated. The load-displacement-time data for each test was exported for unloading fits to the VEP (viscous-elastic-plastic) model (Section 4.3.2). For indentations in bone, a Poisson's ratio of $\nu = 0.3$ was assumed [Zysset et al, 1999] for calculating elastic modulus (*E*) from plane strain modulus (*E*').

Indentation traces for the healing bone samples demonstrated substantial point-to-point variation. Three experimental traces from the same region of the same sample are shown in Figure 4-13 (left) as open symbols. The unloading displacement-time (*h*-*t*) data for each curve were fit to Equation 4-34 and the loading response then predicted from Eqn 4-31 based on the obtained fitting parameters. The complete VEP load-displacement (*P*-*h*) traces are illustrated by the solid lines in Figure 4-13 (right), demonstrating that the experimental bone indentation data were well-described by the VEP model.

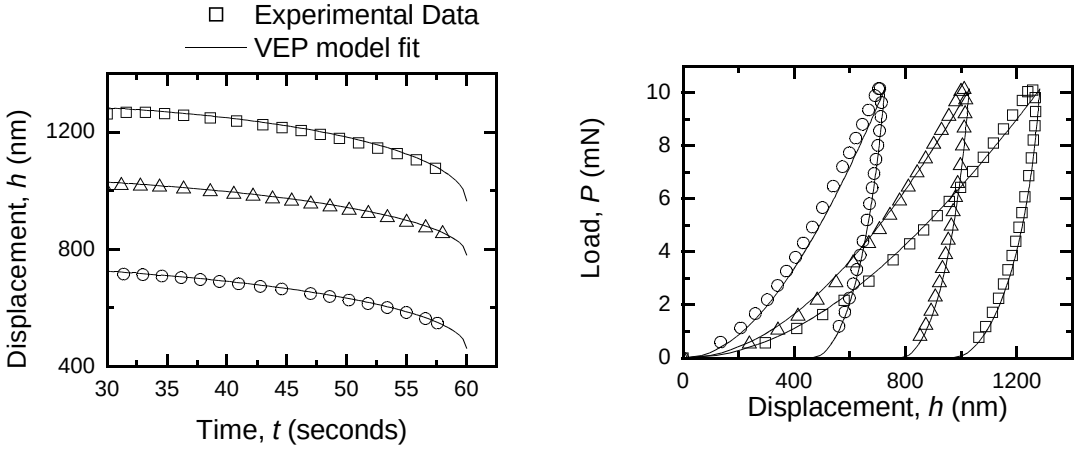

Fig. 4-13 (left) Displacement-time (*h*-*t*) traces for the unloading segment of three indentation tests on healing bone. Experimental data for three different locations on the sample are shown as open symbols; solid lines are fits to Eqn. 4-34. (right) Experimental load-displacement (*P*-*h*) responses for both loading and unloading responses of the same three indentation tests as above (open symbols). The solid lines were generated from the VEP model (Eqns 4-31 and 4-34) using the parameters obtained in the fits.

Variation in the VEP properties (E, H, η_Q) is shown as a function of distance from the bone-implant interface in Figure 4-14. There were variations with indent location over an order of magnitude for *E* and *H*, and over two orders of magnitude for η_Q. The average elastic modulus for all indents was 21.6 GPa. There was a trend for increasing property values with increased distance from the bone-implant interface for

both E and η_Q ($p = 0.02$ and $p < 0.01$ respectively for linear regression in logarithmic coordinates), but no trend for plastic deformation resistance H ($p = 0.893$).

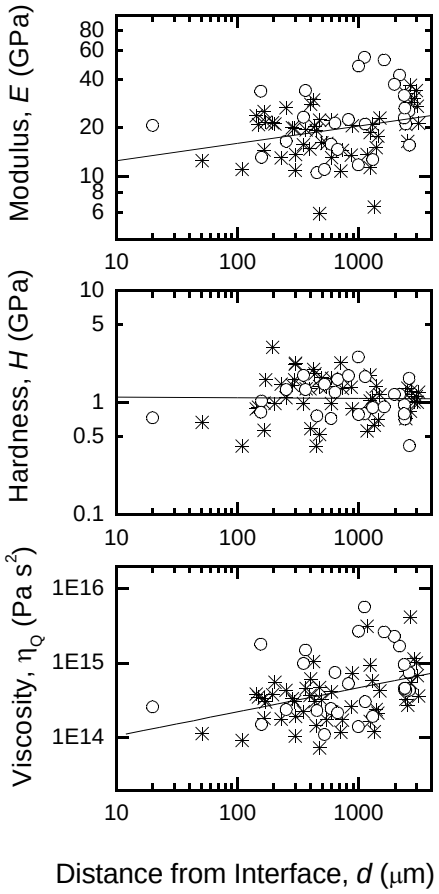

Figure 4-14 VEP model fitting parameters as a function of distance *d* from the bone-implant interface in two porcine samples: (top) modulus *E*; (middle) plastic deformation resistance *H;* (bottom) indentation viscosity η_Q. All three properties demonstrated substantial variability in both animals (individual animals shown as different symbols, o and *).

A graphical representation was used to examine the variability in bone indentation VEP parameters. Representative indentation traces were constructed by inputting the mean properties from Figure 4-14 (viscosity, modulus, and hardness) into the VEP model (Eqns 4-31 and 4-34). Variation in each parameter was assessed by holding two of the

three parameters fixed to the mean value obtained in the current study, and varying the third parameter to the minimum and maximum values obtained in the study. The mean representative response is shown as the solid line in Figure 4-15.

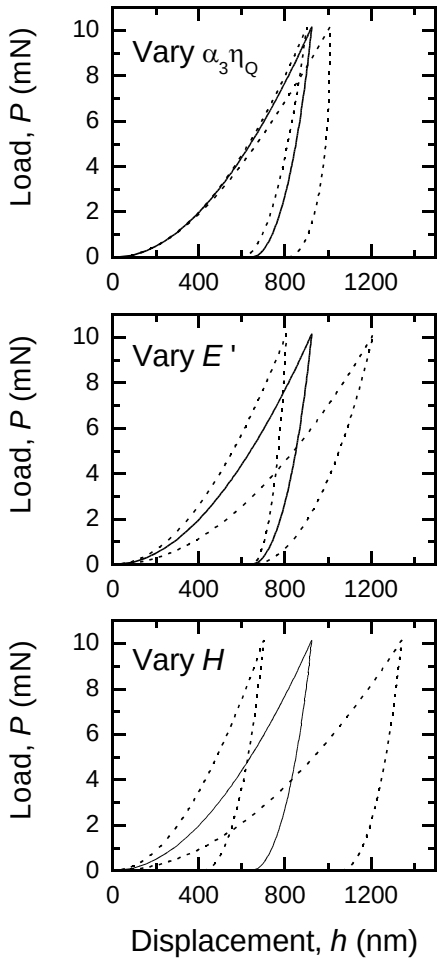

Fig. 4-15 Graphical representation of the range of indentation responses obtained in the current study. The VEP response corresponding to the average modulus, plastic deformation resistance, and viscosity terms from all samples is represented by the solid curve in each graph. Holding the other two parameters fixed, the (top) viscosity, (middle) modulus, and (bottom) plastic deformation resistance is varied over the range of values obtained from fits in the current study. The dotted lines in each plot represent the minimum and maximum values for the varied parameter.

The dotted lines in Figure 4-15 demonstrate the variability in indentation load-displacement response due to variations in each property. The most substantial variation in the current study was due to differences in plastic deformation resistance (H), and the least amount of variation was due to differences in time-dependence.

In this study, the mechanical properties varied substantially with indent location in samples of healing bone. An iterative curve fitting technique was used to calculate three different indentation properties using only the unloading displacement-time response from a constant loading- and unloading-rate indentation test. The curve-fit technique, adapted from a viscous-elastic-plastic indentation model, allowed for simple calculation of material parameters for each indentation test.

The average elastic modulus obtained from the VEP model, 21.6 GPa, was in good agreement with previously reported values for dry bone [Rho et al, 1997] even though the modulus was obtained via a different (Oliver-Pharr) property deconvolution model. The value also agrees well with the Oliver-Pharr modulus seen for elastic-plastic analysis of a subset of these same tests, 17.9 GPa (section 3.2.2). Both Oliver-Pharr analysis and the VEP model are based on the same elastic contact mechanics, so this agreement in elastic modulus would be anticipated for the two approaches.

Both the VEP model itself and the implementation of large-scale use of the model via a fit to the unloading data show great promise for analysis of indentation in time-dependent materials. The ability to measure this time-dependence directly by indentation is a great improvement over techniques aimed at purely removing time-dependence and measuring modulus only [Chudoba and Richter, 2001; Fan and Rho, 2003].

4.4.3 Implications of Viscosity-Modulus Correlations

The use of a model such as VEP allows for indentation analysis of both the forward and reverse problems in indentation [Dao et al, 2001]. That is, the model can both be used to extract parameters from experimental data (Figure 4-14) as well as to

generate indentation traces given a set of input mechanical parameters, as shown in Figure 4-15. This capability will be used next to examine some implications for performing Oliver-Pharr analysis on time-dependent materials.

The experimental data indentation data for bone, presented in Figure 4-14, are characterized by an interesting relationships between two of the parameters. The indentation viscosity, η_Q, was found to be directly related to, and nearly a quadratic function of, the elastic modulus (power law of 1.82, Figure 4-16). This result has interesting experimental implications for indentation analysis of materials with a small to moderate degree of time-dependence, such as cases in which the unloading data do not present an obvious forward displacing unloading "nose" (Figure 4-2). In such cases, many authors would use Oliver-Pharr analysis to extract mechanical parameters, assuming that creep was not dominant in the indentation data.

A VEP loading- and unloading- load-displacement trace was generated for the same plastic deformation resistance (H = 0.67 GPa), and for which a base response is compared with a response for doubled plane strain modulus (E' = 10 or 20 GPa) and a corresponding quadrupled viscosity (η_Q ~ 1e14 or 4e14 Pa-s^2), following the approximate relationship observed in Figure 4-16. The numerical values of the parameters were chosen to be representative of the results seen in the bone study presented in the previous section. These two VEP-generated load-displacement traces are shown as the open symbols in Figure 4-17.

As shown by the solid line approximations to the unloading stiffness (slope), the stiffness (S) is unchanged in these two cases. In Oliver-Pharr deconvolution, the unloading slope (S) is used directly to calculate the plane strain modulus (Eqn. 2-15) where A is the contact area. The data shown in Figure 4-17 can be deconvoluted using Oliver-Pharr analysis, which leads to apparent modulus values that differ by only a factor of 1.2 (instead of two). Since the "elastic" unloading stiffnesses (S) are approximately equal, the apparent modulus difference would be entirely due to the slightly larger contact area (A), resulting from larger total displacement in the case of the E' = 10 GPa curve.

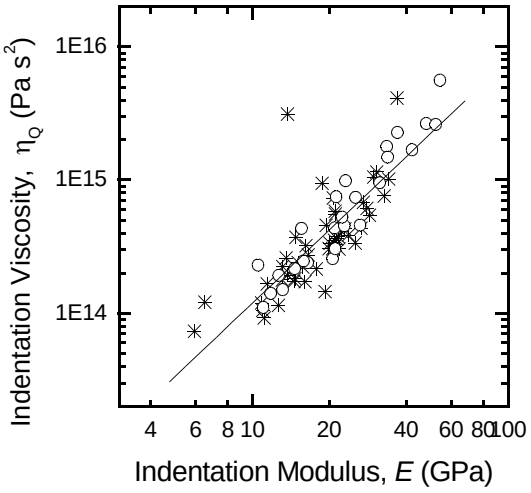

Figure 4-16 Illustration of the direct relationship between VEP viscosity (η_Q) on modulus *E*. The relationship was nearly quadratic (power law factor 1.82).

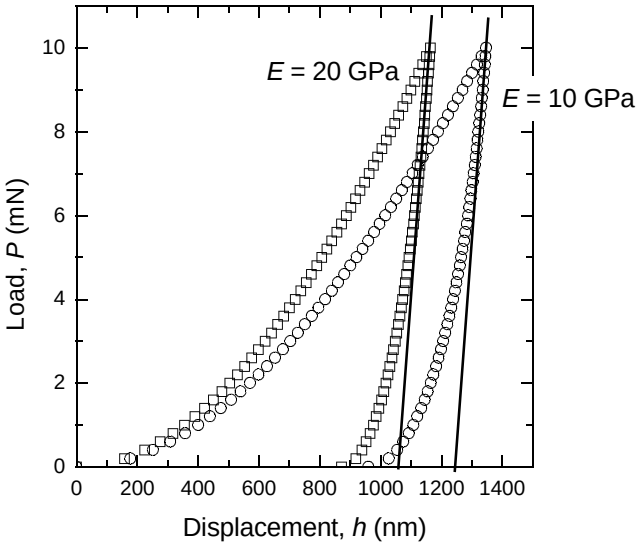

Fig. 4-17 Two indentation load-displacement (*P*-*h*) traces generated from the VEP model for plane strain modulus (*E*') values of 10 and 20 GPa and corresponding viscosity values based on the data shown in Fig. 4-16. The interactions of *E* and η_Q result in an apparent equivalence of the unloading stiffness *S* in these two responses.

Thus, even in the absence of an obvious viscoelastic "nose" (forward deformation on initial unloading), viscous deformation can substantially alter the perceived indentation mechanical properties when Oliver-Pharr analysis is used, in this case, substantially *underestimating* differences in elastic modulus values. Put another way, ignoring the viscosity actually decreases the perceived variability using this analysis.

4.4.4 VEP Comparison of Bone and Dentin

There were interesting differences between the indentation responses of mineralized tissues with similar compositions, bone and dentin, as shown in the elastic-plastic indentation data presented in sections 3.3 and 3.4. A further comparison of these two materials, based on VEP analysis, is presented here.

A series of raw load-displacement (*P*-*h*) responses for bone and dentin, both tested dry and under the same indentation protocol (P_{max} = 10 mN, t_R = 30 seconds), are shown in Figure 4-18. (The bone data here are a subset of that presented in section 4.4.2 above, chosen to be representative such that the averages here for the seven samples are comparable to the overall averages for the whole study of 75 samples. The dentin data are different than those reported in section 4.4.1 due to the rise time differnce.) As has been illustrated previously in this work, dentin responses seem to vary little from point-to-point while bone responses show tremendous local variations in response. The dentin responses also show uniformly smaller peak displacement values than bone under the same loading conditions—there is less total deformation in dentin than in bone. Also shown in Figure 4-18 are the traces following normalization by the peak point. The bone response for one of test shown in Fig. 4-18 is somewhat comparable in shape to the dentin responses, especially on unloading. The remaining bone responses are different in the shape of both the loading and unloading responses.

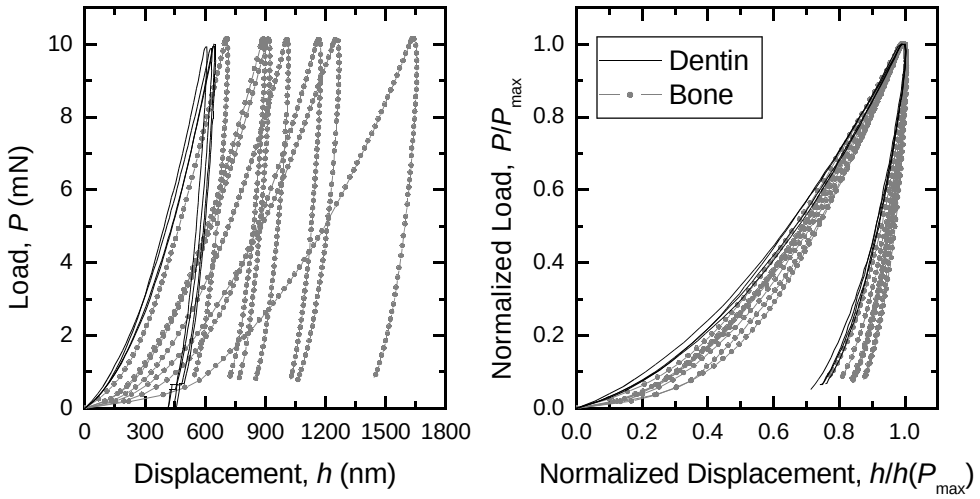

Figure 4- 18: (left) Load-displacement (*P*-*h*) traces for bone and dentin, both dry, tested under the same conditions (10 mN-30s). (right) Normalized load-displacement traces ($h/h(P_{max})$, P/P_{max}) for the bone and dentin data on the left.

The values of parameters obtained from the raw load-displacement responses can also be compared. The mean VEP properties for bone and dentin are shown in Table 4-3 for the data presented in Figure 4-18. The overall trend to much smaller total displacements in the dentin responses (Figure 4-18) are associated with modulus values about one and a half times those of bone, plastic deformation resistance parameters about doubled those of bone, and time-constants about doubled those of bone. This is extremely interesting given the similarities of composition of bone and dentin; no composite materials model would predict such large changes in the raw parameters based merely on the <10% mineral volume fraction difference between the two materials. Structural arrangements of mineral appears to be a potential factor (as will be discussed in Chapter 5).

Table 4-3: Averages of parameters obtained for the VEP fits of load-displacement (*P*-*h*) data shown in Fig. 4-23. (4 dentin, 7 bone indentations)

	Dentin	***Bone***
Plane strain modulus, E' (GPa)	33.3	20.1
Plastic deformation resistance, H (GPa)	3.43	1.17
Indentation (VEP) viscosity, $10^{-15}\eta_Q$ (Pa s^2)	2.0	0.3
Indentation time constant, τ_Q (s)	215.6	111.8
Calculated contact hardness, H_c (GPa)*	0.99	0.40

** see Appendix B*

Another interesting application of the VEP model is an examination of deformation partitioning. From the average VEP properties (Table 4-3) the amounts of raw viscous, elastic, and plastic deformation (h_V, h_E, h_P) can be calculated using Eqns 4-24 to 4-26. The partitioning of deformation components can be assessed by computing the percentage of total deformation from each deformation mode. These deformation components, in both nm and %, are shown in Table 4-4 for dentin, bone and PL-1 polymer (from section 4.3.2), all tested under the same conditions (10 mN, 30 s) as calculated from the property results shown in Tables 4-1 and 4-3. Although the raw parameters differ, the responses for bone and dentin are quite similar in balance of deformation, with plastic deformation dominating the total. The polymer response was dominated by elastic deformation. The time-dependence of all three materials was small but not insignificant under these loading conditions.

Table 4-4: Average deformation components calculated from the VEP data shown in Tables 4-1 and 4-3.

	PL-1 polymer	***Dentin***	***Bone***
Viscous deformation	83 nm (6.0%)	21 nm (3.3%)	55 nm (5.6%)
Elastic deformation	814 nm (58.7%)	261 nm (41.6%)	336 nm (34.2%)
Plastic deformation	489 nm (35.3%)	345 nm (55.1%)	591 nm(60.2%)
Total deformation	1386 nm	627 nm	982 nm

4.5 Discussion

A relatively recent area of research is the development of techniques for characterizing materials with time-dependent mechanical responses using indentation. The hallmarks of time-dependent nanoindentation creep responses were presented here, along with issues that can arise when time-dependence is neglected. Two techniques for analysis of indentation in viscoelastic materials were examined: Radok elastic-viscoelastic correspondence best suited for spherical indenter tips, and an empirical viscous-elastic-plastic (VEP) model exclusively for pyramidal indenter tips.

In this chapter, time-dependent indentation behavior was demonstrated in mineralized tissues, particularly bone and dentin, along with polymeric materials with well-established viscoelastic behavior. The effect of hydration on dentin behavior was illustrated, along with the point-to-point variations in bone responses. In hydrated samples, responses for dentin were found to be more variable than for dehydrated samples (section 4.4.1). There was a large difference between VEP and Oliver-Pharr deconvolution for hydrated samples, but little difference for dry samples.

Another interesting result from the current examination of dry bone behavior in particular is that the time-dependence may actually smooth out variability in Oliver-Pharr (unloading stiffness-based) elastic modulus results, not increase the variability (section 4.4.3). Therefore, for the dry bone data presented in Chapter 3, it does not appear that hydration or dominant time-dependent behavior are the effects causing indentation variability—both hydration and direct accounting for viscosity actually added to the perceived variability. These factors are not likely interfering with the ability to detect trends with respect to healing time or distance from the bone-implant interface in the dental implant study. Therefore, further examinations of mineralized tissue ultrastructure-mechanics relationships in the remainder of this work will emphasize elastic mechanical behavior, with an emphasis on structural and compositional variations as opposed to viscoelastic effects.